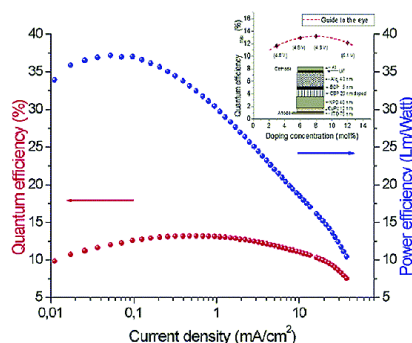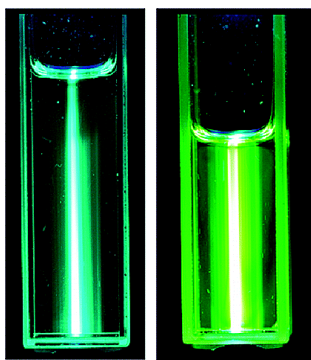**Article**

Highly Phosphorescence Iridium Complexes and Their Application in Organic Light-Emitting Devices

Md. K. Nazeeruddin, R. Humphry-Baker, D. Berner, S. Rivier, L. Zuppiroli, and M. Graetzel

More About This Article

Additional resources and features associated with this article are available within the HTML version:

- Supporting Information
- Links to the 54 articles that cite this article, as of the time of this article download
- Access to high resolution figures
- Links to articles and content related to this article
- Copyright permission to reproduce figures and/or text from this article

View the Full Text HTML

Highly Phosphorescence Iridium Complexes and Their Application in Organic Light-Emitting Devices

Md. K. Nazeeruddin,*,† R. Humphry-Baker,† D. Berner,§ S. Rivier,‡ L. Zuppiroli,‡ and M. Graetzel†

Contribution from the Laboratory for Photonics and Interfaces, Institute of Physical Chemistry, Swiss Federal, Institute of Technology, CH-1015 Lausanne, Switzerland, Laboratoire d'Optoélectronique des Matériaux Moléculaires, Institut des Matériaux, Ecole Polytechnique Fédérale, CH-1015 Lausanne, Switzerland, and CFG Microelectronic, CH-1110 Morges, Switzerland

Received December 5, 2002; Revised Manuscript Received March 14, 2003 ; E-mail: MdKhaja.Nazeeruddin@epfl.ch

Abstract: A new series of iridium(III) mixed ligand complexes TBA[Ir(ppy)$_2$(CN)$_2$] (**1**), TBA[Ir(ppy)$_2$(NCS)$_2$] (**2**), TBA[Ir(ppy)$_2$(NCO)$_2$] (**3**), and [Ir(ppy)$_2$(acac)] (**4**) (ppy = 2-phenylpyridine; acac = acetoylacetonate, TBA = tetrabutylammonium cation) have been developed and fully characterized by UV−vis, emission, IR, NMR, and cyclic voltammetric studies. The lowest energy MLCT transitions are tuned from 463 to 494 nm by tuning the energy of the HOMO levels. These complexes show emission maxima in the blue, green, and yellow region of the visible spectrum and exhibit unprecedented phosphorescence quantum yields, 97 ± 3% with an excited-state lifetimes of 1−3 μs in dichloromethane solution at 298 K. The near-unity quantum yields of these complexes are related to an increased energy gap between the triplet emitting state and the deactivating e$_g$ level that have been achieved by meticulous selection of ligands having strong ligand field strength. Organic light-emitting devices were fabricated using the complex **4** doped into a purified 4,4′-bis(carbazol-9-yl)biphenyl host exhibiting a maximum of the external quantum efficiencies of 13.2% and a power efficiency of 37 lm/W for the 9 mol % doped system.

1. Introduction

The photophysical and photochemical properties of d^6 ruthenium(II), osmium(II), rhenium(I), rhodium(III), and iridium-(III) have been thoroughly investigated during the last 2 decades.[1−3] The main thrust behind these studies is to understand the energy and electron transfer processes in the excited state and to apply this knowledge to potential practical applications such as in solar energy conversion,[4] organic light-emitting diodes,[5−8] electroluminescence,[9,10] and sensors.[11,12] Application of panchromatic d^6 ruthenium and osmium complexes in dye-sensitized solar cells yielded near-unity incident photon-to-current conversion efficiency (IPCE).[13,14] However, utilization of ruthenium(II) complexes in light-emitting devices offered electron to photon conversion efficiency of 5.5%.[7,15] In these devices holes and electrons are injected by opposite electrodes, which migrate to an internal interface and recombine to form excited states that can be nonradiative or radiative singlet or triplet in nature. The highest phosphorescence quantum yields reported for ruthenium complexes containing substituted 2,2′-bipyridine and 1,10-phenanthroline ligands at 298 K are around 40%.[1]

One of the main requirements for organic light-emitting diodes (OLED) is that the complex should exhibit very high phosphorescence quantum efficiencies. Iridium(III) complexes containing 2-phenylpyridine are known to exhibit high triplet quantum yields due to mixing the singlet and the triplet excited states via spin−orbit coupling, which enhances the triplet-state subsequently, leading to high phosphorescence efficiencies.[16−18] Several groups have used extensively Ir(III)-based sensitizers in light-emitting devices and obtained up to 12.3% external quantum efficiencies.[5,19−23] Therefore, by increasing the sensitizer triplet quantum yields, one would expect to increase the

† Institute of Physical Chemistry, Swiss Federal.

‡ Laboratoire d'opto électronique des matériaux Moléculaires, Institut des Matériaux.

§ CFG Microelectronic.

(1) Juris, A.; Balzani, V.; Barigelletti, F.; Campagna, S.; Belser, P.; von Zelewsky, A. *Coord. Chem. Rev.* **1988**, *84*, 85.
(2) Meyer, T. J. *Acc. Chem. Res.* **1989**, *22*, 163.
(3) Kalyanasundaram, K.; Grätzel, M. *Coord. Chem. Rev.* **1977**, *77*, 347.
(4) Grätzel, M. *Nature* **2001**, *414*, 338.
(5) Adachi, C.; Baldo, M. A.; Forrest, S. R.; Thompson, M. E. *Appl. Phys. Lett.* **2000**, *77*, 6904.
(6) Gao, F. G.; Bard, A. J. *Chem. Mater.* **2002**, *14*, 3465.
(7) Gao, F. G.; Bard, A. J. *J. Am. Chem. Soc.* **2000**, *122*, 7426.
(8) Handy, E. S.; Pal, A. J.; Rubner, M. F. *J. Am. Chem. Soc.* **1999**, *121*, 3525.
(9) Zu, Y.; Bard, A. J. *Anal. Chem.* **2001**, *73*, 3960.
(10) Lee, J. K.; Yoo, D.; Rubner, M. F. *Chem. Mater.* **1997**, *9*, 1710.
(11) Amao, Y.; Ishikawa, Y.; Okura, I. *Anal. Chim. Acta* **2001**, *445*, 177.
(12) Zakeeruddin, S. M.; Fraser, D. M.; Nazeeruddin, M. K.; Grätzel, M. *J. Electroanal. Chem.* **1993**, *337*, 2536.

(13) Nazeeruddin, M. K.; Pechy, P.; Renouard, T.; Zakeeruddin, S. M.; Humphry-Baker, R.; Comte, P.; Liska, P.; Le, C.; Costa, E.; Shklover, V.; Spiccia, L.; Deacon, G. B.; Bignozzi, C. A.; Graetzel, M. *J. Am. Chem. Soc.* **2001**, *123*, 1613.
(14) Kuciauskas, D.; Freund, M. S.; Gray, H.; Winkler, J. R.; Lewis, N. S. *J. Phys. Chem. B* **2001**, *105*, 392.
(15) Rudmann, H.; Shimada, S.; Rubner, M. F. **2001**, *124*, 4918.
(16) Wang, Y.; GHerron, N.; Grushin, V. V.; LeCloux, D.; Petrov, V. *Appl. Phys. Lett.* **2001**, *79*, 449.
(17) Ohsawa, Y.; Sprouse, S.; King, K. A.; DeArmond, M. K.; Hanck, K. W.; Watts, R. J. *J. Phys. Chem.* **1987**, *91*, 1047.
(18) Garces, F. O.; King, K. A.; Watts, R. J. *Inor. Chem.* **1988**, *27*, 3464.

efficiency of light-emitting diodes. Nevertheless, achieving room-temperature phosphorescence quantum efficiency close to unity using transition metal complexes remained as a challenge in the field of inorganic photochemistry. In this paper we report the synthesis and characterization of tailored iridium mixed ligand complexes, which show phosphorescence quantum yields close to unity with excited-state lifetimes of $1-3$ μs in dichloromethane solution at 298 K. Also we demonstrate the tuning aspect of MLCT transitions to achieve blue, green, and yellow emission colors.

2. Experimental Section

2.1. Materials. The solvents (puriss grade), tetrabutylammonium cyanide, tetrabutylammonium thiocyanate, tetrabutylammonium cyanate, and acetyl acetone were purchased from Fluka. 2-Phenylpyridine ligand and hydrated iridium trichloride were used as received from Aldrich and Johnson Matthey, respectively. Sephadex LH-20 (Pharmacia) was allowed to swell in methanol for 12 h before loading into a 3 × 50-cm column. The dichloro-bridged iridium dimer [Ir(ppy)$_2$-(Cl)]$_2$ was synthesized using a reported procedure.[18]

2.2. Analytical Measurements. UV−vis spectra were recorded in a 1 cm path length quartz cell on a Cary 5 spectrophotometer. Emission spectra were recorded on a Spex Fluorolog 112 using a 90° optical geometry. The emitted light was detected with a Hamamatsu R2658 photomultiplier operated in single photon counting mode. The emission spectra were photometrically corrected using a NBS-calibrated 200-W tungsten lamp as reference source. A dilute solution of recrystallized quinine sulfate in 1 N H$_2$SO$_4$ was used as a quantum yield standard.[22] A secondary standard using recrystallized Ru(bpy)$_3$(PF$_6$)$_2$ solution was also employed to verify the yields.[24] The emission lifetimes were measured by exciting the nitrogen-purged sample with a pulse from an active mode-locked Nd:YAG laser, using the frequency tripled line at 355 nm. The emission decay was followed on a Tektronix DSA 640 digitizing signal analyzer, using a Hamamatsu R928 photomultiplier to convert the light signal to a voltage waveform. The solutions were prepared to give approximate concentrations of 1 μM.

The thin films containing iridium complexes were prepared by blending 1% (by weight) of the required complex into poly(methacrylic acid methyl ester) polymer. The photoluminescence quantum yields of the dyes in a thin film were measured using an integrating sphere coupled to the spectrofluorimeter. A Kr ion laser excitation source was used to irradiate the sample at 468.04 nm. The procedure employed was to measure the spectral response of the sphere under three configurations. First the sphere is empty and a background response of the sphere is recorded using the laser light source. Next the sample is placed in the sphere but out of the laser beam so as to measure the emission contribution from the diffuse laser light. Last, the sample is excited directly. The emission quantum yield is then extracted from these three spectra using an approach analogous to that of Friend et al.[25]

Electrochemical data were obtained by cyclic voltammetry using a three-electrode cell and an Auto lab system (PGSTAT 30, GPES 4.8 software). The working electrode was a 0.03 cm^2 glassy carbon disk, the auxiliary electrode was a glassy carbon rod, and a silver disk of 0.03 cm^2 was used as quasireference electrode. Tetrabutylammonium

tetrafluoroborate (TBATFB, 0.1 M) was used as supporting electrolyte in dichloromethane solution. Ferrocene was added to each sample solution at the end of the experiments and the ferrocenium/ferrocene redox couple was used as an internal potential reference.

^{1}H and ^{13}C NMR spectra were measured with a Bruker ACP-200 spectrometer at 200 MHz and 50.3 MHz, respectively. The reported chemical shifts were against TMS. The ATR-FTIR spectra for all the samples were measured using a Digilab 7000 FTIR spectrometer. The FTIR data reported here was taken with the "Golden Gate" diamond anvil ATR accessory (Graseby-Specac) using typically 64 scans at a resolution of 2 cm^{-1}. The samples were all measured under the same mechanical force pushing the samples in contact with the diamond window. No ATR correction has been applied to the data.

2.3. Organic Light-Emitting Device. The general architecture of the complex multilayer diodes used in this study is as follows: The ITO (indium−tin oxide) coated glass substrates (30 Ω/□, Applied Film Corp.) were first cleaned in ethanol, acetone, and soap ultrasonic baths. Then the ITO electrodes were covered by a 10 nm thick CuPc (copper phthalocyanine) layer for hole injection improvement. Next a 40 nm layer of α-NPD (N,N′-diphenyl-N,N′-bis(1-naphthyl)-1,1′-biphenyl-4,4″-diamine) was evaporated as a hole-transporting layer, followed by a 20 nm layer of CBP (4,4′-bis(carbazol-9-yl)biphenyl) as a wide band gap emitting matrix coevaporated with different rates of 0, 3, 6, 9, and 12 mol % of the phosphorent emitter molecule (ppy)$_2$Ir(acac) (bis(2-phenylpyridine)iridium(III) acetylacetonate). For hole blocking and resulting charge confinement in the emitting matrix layer we used a 5 nm layer of BCP (2,9-dimethyl-4,7-diphenylphenatroline), and for the electron transport layer we used a 40 nm layer of Alq$_3$ (tris(8-hydroxy-quinolato)aluminum). All organics were purified by gradient sublimation and thermally evaporated at a rate of 1.0 Å/s at a base pressure of around 3.5 × 10^{-7} Torr. A 0.8 nm LiF layer was then deposited right after the Alq$_3$, at a rate of 0.2 Å/s. The finishing Al electrode (cathode) was deposited at a rate of 10 Å/s in another chamber without breaking the vacuum. The active area of the diode segments was 12 mm^2.

The current versus voltage $I(V)$ characteristics of each device were measured in a nitrogen atmosphere glovebox by means of a LabView controlled Keithley 236 measuring unit. Simultaneously, the light output was measured by a photodiode, calibrated with a Minolta LS110 luminance meter.

2.4. Synthesis. 2.4.1. Synthesis of TBA[Ir(ppy)$_2$(CN)$_2$] (1). The dimeric iridium(III) complex [Ir(ppy)$_2$(Cl)]$_2$ (178 mg) was dissolved in 30 mL of dichloromethane solvent under nitrogen. To this solution was added tetrabutylammonium cyanide (534 mg) ligand. The reaction mixture was refluxed with stirring for 15 h. Then, to the solution was added a 1:1 solvent mixture of diethyl ether and low-boiling petroleum ether (60 mL). The precipitated solid was collected and recrystallized from methanol and low-boiling petroleum ether. The air-dried product weighed 230 mg (yield 87%).

Anal. Calcd for TBA[Ir(ppy)$_2$(CN)$_2$]: C, 60.43; H, 6.59; N, 8.80. Found: C, 60.27; H, 6.60; N, 8.73.

^{1}H NMR 200 MHz, (DMSO-d_6) δ ppm: 0.93 (12H, t, CH$_3$), 1.29 (8H, q, CH$_2$), 1.48 (8H, m, CH$_2$), 3.15 (8H, t, CH$_2$), 6.08 (2H, d, J = 7.2), 6.60 (2H, t, J = 7.1), 6.73 (2H, t, J = 7.2), 7.3 (2H, t, J = 7.2), 7.65 (2H, d, J = 7.4), 7.89 (2H, t, J = 7.3), 8.07(2H, d, J = 7.8), 9.53 (2H, d, J = 5.9).

^{13}C NMR 200 MHz, (DMSO-d_6) δ ppm: 170.2, 163.42, 154.97, 145.83, 139.76, 137.44, 132.17, 129.64, 124.72, 123.36, 121.62, 120.11, 59.49, 24.77, 20. 70, 13.93.

2.4.2. Synthesis of TBA[Ir(ppy)$_2$(NCS)$_2$] (2). Using the same conditions as for complex **1**, starting from the dimeric iridium(III) complex and tetrabutylammonium thiocyanate, the title compound was obtained as a yellow powder (yield 72%).

Anal. Calcd for TBA[Ir(ppy)$_2$(NCS)$_2$]: C, 55.92; H, 6.09; N, 8.15; S, 7.46. Found: C, 55.94; H, 5.95; N, 7.96; S, 7.96.

^{1}H NMR 200 MHz, (DMSO-d_6) δ ppm: 0.98 (12H, t, CH$_3$), 1.28 (8H, q, CH$_2$), 1.49 (8H, m, CH$_2$), 3.19 (8H, t, CH$_2$), 5.95 (2H, d, J =

(19) Baldo, M. A.; Lamansky, S.; Burrows, P. E.; Thompson, M. E.; Forrest, S. R. *Appl. Phys. Lett.* **1999**, *75*, 4.
(20) Ikai, M.; Tokito, S.; Sakamoto, Y.; Suzuki, T.; Taga, Y. *Appl. Phys. Lett.* **2001**, *79*, 156.
(21) Lee, C.-L.; Lee, K. B.; Kim, J.-J. *Appl. Phys. Lett.* **2000**, *77*, 2280.
(22) Tsutsui, T.; Yang, M.-J.; Yahiro, M.; Nakamura, K.; Watanabe, T.; Tsuji, T.; Fukuda, Y.; Wakimoto, T.; Miyaguchi, S. *Jpn. J. Appl. Phys.* **1999**, *38*, L1502.
(23) Wang, Y.; Herron, N.; Grushin, V. V.; LeCloux, D.; Petrov, V. *Applied Physics Lett.* **2001**, *79*, 449.
(24) Nakamaru, K. *Bull. Chem. Soc. Jpn.* **1982**, *55*, 2697.
(25) Mello, J. C.; Wittmann, H. F.; Friend, R. H. *Adv. Mater.* **1997**, *9*, 230.

7.4), 6.59 (2H, t, *J* = 7.2), 6.74 (2H, t, *J* = 7.7), 7.5 (2H, t, *J* = 7), 7.66 (2H, d, 7.9), 7.98 (2H, t, *J* = 7.1), 8.14 (2H, d, *J* = 7.5), 9.08 (2H, d, *J* = 5.5).

^{13}C NMR 200 MHz, (DMSO-*d6*) δ ppm: 167.7, 150.32, 150.01, 144.91, 137.99, 131.33, 129.03, 128.76, 124.22, 123.07, 120.79, 119.33, 58.29, 23.87, 20.01, 13.93.

2.4.3. Synthesis of TBA[Ir(ppy)2(NCO)2] (3). Using the same conditions as for complex **1**, starting from the dimeric iridium(III) complex and tetrabutylammonium cyanate the title compound was obtained as a dark yellow powder (yield 69%).

Anal. Calcd for TBA[Ir(ppy)2(NCO)2]: C, 58.09; H, 6.33; N, 8.46. Found: C, 57.43; H, 6.22; N, 8.41.

^{1}H NMR 200 MHz, (DMSO-*d6*) δ ppm: 0.93 (12H, t, CH3), 1.30 (8H, q, CH2), 1.52 (8H, m, CH2), 3.19 (8H, t, CH2), 5.98 (2H, d, *J* = 6.5), 6.51 (2H, t, *J* = 6.1), 6.67 (2H, t, *J* = 7.2), 7.36 (2H, t, *J* = 5.9), 7.58 (2H, d, 6.7), 7.86 (2H, t, *J* = 7.5), 8.05 (2H, d, *J* = 8), 9.25 (2H, d, *J* = 5.6).

^{13}C NMR 200 MHz, (DMSO-*d6*) δ ppm: 168.17, 150.49, 145.03, 139.68, 138.74, 138.94, 131.53, 128.58, 123.89, 122.25, 119.52, 116.55, 57.86, 23.40, 19.57, 13.83.

2.4.4. Synthesis of [Ir(ppy)2(acac)] (4). This complex was synthesized with slight modification of a reported procedure.[26] Acetyl acetone (80 mg) was dissolved in 0.5 mL of ethanol and was added to a solution of dimeric iridium(III) complex (340 mg), which was predissolved in 25 mL of dichloromethane. Then, tetrabutylammonium hydroxide (207 mg) was introduced into the reaction mixture and was refluxed for 5 h, after which the solution was evaporated to dryness and the resulting solid was collected on a sintered glass crucible and washed thoroughly with ethanol. The yield of the dried product was 90%.

Anal. Calcd for [Ir(ppy)2(acac)] (**4**): C, 54.08; H, 3.87; N, 4.67; Found: C, 54.16; H, 3.94; N, 4.72.

^{1}H NMR 200 MHz, (DMSO-*d6*) δ ppm: 1.71 (6H, s, CH3), 5.25 (1H, s CH), 6.05 (2H, d, *J* = 7.4), 6.59 (2H, t, *J* = 7.4), 6.78 (2H, t, *J* = 7.4), 7.38 (2H, t, *J* = 7), 7.68 (2H, d, 7.5), 7.93 (2H, t, *J* = 7.5), 8.13 (2H, d, *J* = 7.8), 8.42 (2H, d, *J* = 5.3).

^{13}C NMR 200 MHz, (DMSO-*d6*) δ ppm: 184.31, 167.90, 148.10, 147.73, 145.41, 138.24, 132.94, 128.87, 124.29, 122.78, 120.85, 119.19, 100.84, 57.86, 26.57.

3. Results and Discussion

3.1. Synthetic Studies. The iridium pseudohalogen complexes were synthesized under inert atmosphere by reacting the dichlorobridged iridium dimer [Ir(ppy)2(Cl)]2 in dichloromethane solvent with an excess of a pseudohalogen ligand such as tetrabutylammonium cyanide, tetrabutylammonium thiocyanate, or tetrabutylammonium cyanate, which gave over 70% yields of the anionic TBA[Ir(ppy)2(CN)2] (**1**), TBA[Ir(ppy)2(NCS)2] (**2**), and TBA[Ir(ppy)2(NCO)2] (**3**) complexes, respectively. The complex [Ir(ppy)2(acac)] (**4**) was synthesized by refluxing the dimer and acetyl acetone in the presence of the strong base tetrabutylammonium hydroxide. The crude complexes were purified on a Sephadex LH-20 column using methanol as an eluent. In all the complexes there was a small dull yellow band, which eluted first followed by a bright yellow band. The main bright yellow band was concentrated to 2−3 mL to which was added slowly diethyl ether to crystallize the required complex. Elemental analysis data are consistent with the proposed structures. These complexes are stable at room temperature as a solid and in solution containing noncoordinating solvents such as dichloromethane, chloroform, methanol, or ethanol. However, in strong a coordinating solvent such as dimethyl sulfoxide

(DMSO), only the complex **1** and **4** were stable, but the complexes **2** and **3** undergoes slow substitution of the pseudohalogen ligands upon standing for days in DMSO. The complex **4** was sublimed in a vacuum without any decomposition; the anionic complexes were decomposed during a sublimation process due to heat.

3.2. NMR Spectroscopy. The ^{1}H NMR spectrum of complex **1**, measured in (CD3)2SO solution, displays eight well-resolved signals (four doublets and four triplets) in the aromatic region between 9.7 and 6 ppm, corresponding to the phenylpyridine protons.[27] In the aliphatic region, a triplet centered at 3.15 ppm, two multiplets at 1.48 and 1.29 ppm, and a triplet at 0.93 ppm are assigned to the tetrabutylammonium cation. The complexes **2** and **3** shows similar patterns in the aromatic and the aliphatic region. The integrated ratio between aliphatic protons and aromatic protons in complexes **1**−**3** show the presence of one tetrabutylammonium cation per iridium center, in agreement with the analysis data. The proton NMR data of complexes **1**−**3** clearly show that they are highly symmetric and also show the absence of any corresponding linkage isomers. The iridium metal with two phenylpyridine ligands forms a configuration in which the two pyridine groups are trans to each other and the phenyl groups are trans to the pseudohalogens, resulting in two electronically equivalent pyridines and phenyl groups.[18,27,28] There is no significant change in the NMR spectral pattern between the starting complex [Ir(ppy)2(Cl)]2 and the complexes **1**−**4**, indicating that the cleavage of the chloride bridge and the subsequent substitution of the chloride ligands by pseudohalogens takes place without change in the geometry of the iridium octahedral complex.

The ^{13}C NMR spectrum of complexes **1**−**4** show 12 resonance peaks in the aromatic region in which eleven carbon resonances are due to phenylpyridine and one pseudohalogen/ carbonyl carbon of acetyl acetone. Watts et al. have assigned individual carbon resonances of phenylpyridine ligand in iridium complexes using COSY spectra.[28] Here no attempts were made to deal with individual aromatic carbons. However, the signal at 163.42 ppm in complex **1** is assigned to the coordinated CN ligand by comparing the ^{13}C NMR spectra of **1** with that of the starting [Ir(ppy)2(Cl)]2 complex.[29] In complexes **2** and **3** the carbon signal corresponding to the NCS and NCO ligands were observed at 128.76 and 139.66 ppm, respectively.[13] The striking difference in the peak positions of the CN carbon compared to the NCS and the NCO carbons is due to direct C-coordination of the CN ligand to the metal center, which deshields significantly. Whereas, in the case of NCS or NCO, the coordination is through the nitrogen and, consequently, the carbon atoms are more shielded compared to those of the CN ligand. It is interesting to note the absence of any linkage isomers in iridium-(III) pseudohalogen complexes compared to ruthenium(II) complexes, where 5−10% formation of linkage isomers is evident. In complex **4** the three peaks at 184.3 100.64, and 28.57 ppm are assigned to the acetyl acetone carbons. In the aliphatic region of complexes **1**−**3** there are four resonance peaks due to the tetrabutylammonium group.[13]

3.3. FT-IR Data. Infrared spectra of the compounds **1**−**3** showed the characteristic bands for the coordinated cyanide,

(26) Lamansky, S.; Djurovich, P.; Murphy, D.; Abdel-Razzaq, F.; Kwong, R.; Tsyba, I.; Bortz, M.; Mui, B.; Bau, R.; Thompson, M. E. *Inorg. Chem.* **2001**, *40*, 1704.

(27) Garces, F. O.; Watts, R. J. *Magn. Reson. Chem.* **1993**, *31*, 529.

(28) Graces, F. O.; Dedian, K.; Keder, N. L.; Watts, R. J. *Acta Crystallogr.* **1993**, *49*, 1117.

(29) Kohle, O.; Ruile, S.; Grätzel, M. *Inorg. Chem.* **1996**, *35*, 4779.

Table 1. Absorption and Electrochemical Data of Complexes **1**–**4**

complex	abs. λ_{max}, nm (ϵ, 10^3 M^{-1} cm^{-1})	V vs Fc$^{+/0}$ ^{b}	
		$E_{1/2}$	L/L^{-} ^{c}
1	463 (0.21), 433$_{sh}$ (0.61), 384 (0.58), 337 (0.85), 260 (41.7)	0.91	**−1.7**
2	476 (0.65), 437 (2.3), 400 (3.4), 355 (5.3), 335 (6.7), 300 (16.9), 266 (38.9)	0.45	**−1.95**
3	497 (1.26), 464, (2.36), 408 (3.41), 384 (4.22), 347 (6.62), 276 (35.1)	0.18	**−2.07**
4	492 (1.03), 450 (3.15), 403 (4.76), 356 (8.17), 260 (4.9)	0.46	**−1.72**
[Ir(ppy)$_2$(Cl)]$_2$	484 (0.63), 450 (3.32), 437 (3.5), 403 (5.49) 354 (9.47), 260 (60.1)	0.52 0.78	**−1.71**

^{a} Measured in dichloromethane at 298 K. ^{b} Ferrocene was used in each sample as an internal reference. ^{c} Irreversible reduction wave.

thiocyanate, and cyanate ligands. The FT-IR spectra of complex **1** in the 500−4000 cm^{-1} region display a strong absorption at 2092 cm^{-1} that is assigned to the C-coordinated v(CN). The strong and intense bands at 2099 and 2229 cm^{-1} are due to v(NC) of NCS and the v(NC) of NCO in complex **2** and **3**, respectively. The intensity of the v(NC) in complexes **2** and **3** is at least three times higher than the v(CN) of complex **1**. The NCS^{-} and NCO^{-} groups have two characteristic modes, v(NC) and v(CS/O), which are frequently considered as diagnostic with respect to the coordination mode of the ligand. [30] The observed band positions are in agreement with the N-coordination of the NCS and NCO ligands in these complexes. The ring stretching modes were observed at 1601, 1581, 1470, and 1416 cm^{-1}. The four peaks between 2870 and 2965 cm^{-1} are assigned to the tetrabutylammonium symmetric and asymmetric v(C−H) modes. [31]

3.4. Electrochemical Analysis. The cyclic voltammogram of the dimeric complex [Ir(ppy)$_2$(Cl)]$_2$ measured in dichloromethane containing 0.1 M tetrabutylammonium tetrafluoroborate shows two reversible waves at 0.52 and 0.78 V vs ferrocene due to oxidation of the two iridium metal centers, which is consistent with reported data. [18] The separation between the cathodic and the anodic wave is 130 mV, with a peak current ratio of 0.75. The complexes **1** and **2** show a quasireversible couple at 0.91 and 0.45 V, respectively. The ratio between the cathodic and anodic peak current is 0.21, which decreases further on increasing the scan rate per second. Nevertheless, under identical experimental conditions complex **3** shows a reversible wave at 0.18 V vs ferrocene (Table 1). Changes in the electron-donating or -withdrawing nature of the ligand can result in a variation of electronic properties at the metal center. It is interesting to compare complexes **1** and **3**, which contain cyanide and cyanate ligands, respectively. The 730 mV cathodic shift in oxidation potential of complex **3** compared to complex **1** shows the extent of π back-bonding to the cyanide ligand from the iridium(III) center. The enormous enhancement in π back-bonding leads to a significant blue shift in the low-energy MLCT (metal-to-ligand charge transfer) and the emission maxima of this complex compared to **3**. Complex **4** shows a reversible couple at 0.6 V vs ferrocene. In complexes **1**−**4** no reversible reduction waves in dichloromethane due to phenyl-pyridine ligand were observed. However, significant reduction

(30) Nakamoto, K. *Infrared and Raman Spectra*, 4th ed.; John Wiley & Sons: New York, 1986.
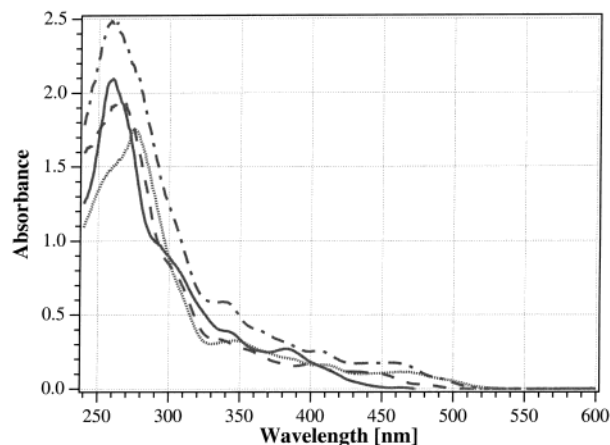(31) Finnie, K. S.; Bartlett, J. R.; Woolfrey, J. L. *Langmuir* **1998**, *14*, 2744.

Figure 1. Absorption spectra of **1** (solid line), **2** (dashed line), **3** (dotted line), and **4** (dashed−dotted line) in degassed dichloromethane solution at 298 K.

currents at above −1.7 V are visible in the cyclic voltammogram, which were not analyzed in detail. [17,18]

3.5. Electronic Spectra. Figure 1 show a comparison of absorption spectra of complexes **1**−**4** measured in dichloromethane solution at 298 K, and the pertinent data are gathered in Table 1. The absorption spectra of these complexes display bands in the UV and the visible region due to intraligand (π−π*) and MLCT transitions, respectively. [32] The low-energy MLCT band in complex **1** (463 nm), significantly blue-shifted compared to those of complexes **2** (478 nm) and **3** (494 nm), indicates the extent of the π-acceptor strength of the CN^{-} ligand compared to the NCS^{-} and NCO^{-} ligands. The spectral shifts are consistent with the electrochemical data of these complexes. Hay in his recent paper has analyzed the spectral properties of iridium(III) phenylpyridine complexes using density functional theory (DFT), in which the low-lying transitions are categorized as metal-to-ligand charge-transfer transitions and the high-energy bands at above 280 nm are assigned to the intraligand π−π* transition of 2-phenylpyridine. [33] It is interesting to note the changes in the molar extinction coefficient of the low-energy MLCT band that in complex **3** is two times higher than that of the thiocyanate complex **2**, which in turn is three times higher than that of the cyanide complex **1**.

3.6. Emission Spectroscopic Data. Figure 2 show a comparison of the emission spectra of complexes **1**−**3** measured in dichloromethane solution at 298 K. Argon-degassed solutions of complexes **1**, **2**, and **3**, when excited within the π−π* and MLCT absorption band at 298 K, show emission maxima at 470, 506, and 538 nm, respectively, with longer lifetimes (0.8−3.4 μs). In contrast, air-equilibrated dichloromethane solutions exhibit short luminescence lifetimes (70−90 ns). It is exciting to note that the argon-degassed dichloromethane solution of these complexes show bright luminescence in a lighted room. Even in the solid state the complexes are highly luminescent, but the emission maximum is slightly red-shifted compared to the solution spectra. The photoluminescence maxima and the quantum yields of thin films containing iridium complexes **1**−**3** were measured using an integrating sphere and are collected in Table 2. Figure 3 shows a schematic representation of highest occupied and lowest unoccupied molecular orbitals of complexes

(32) Schmid, B.; Garces, F. O.; Watts, R. J. *Inorg. Chem.* **1994**, *33*, 9.
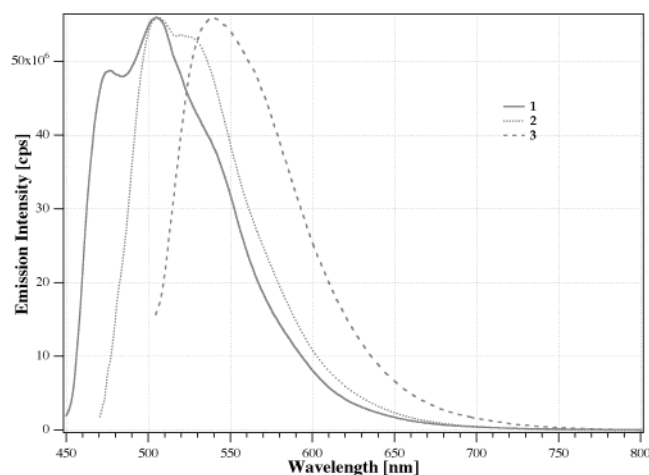(33) Hay, P. J. *J. Phys. Chem. A* **2002**, *106*, 1634.

Figure 2. Emission spectra of **1** (solid line), **2** (dotted line), and **3** (dashed line) in degassed dichloromethane solution at 298 K.

Table 2. Emission, Lifetime, and Quantum Yields Data of Complexes **1**−**4** Measured at 298 K

complex	solvent	emis λ_{max}, nm[a]	emis $\varnothing_f$	solid-state emis λ_{max}, nm	solid-state emis $\varnothing_f$	lifetime (τ), μs
1	CH$_2$Cl$_2$	470, 502	0.94 ± 0.05	500	0.75 ± 0.1	3.14 ± 0.5%
1	CH$_3$CN	470, 502	0.79 ± 0.1			
2	CH$_2$Cl$_2$	506, 520	0.97 ± 0.05	506	0.78 ± 0.1	1.43 ± 0.5%
2	CH$_3$CN	506, 520	0.99 ± 0.05			
3	CH$_2$Cl$_2$	538, 560	0.99 ± 0.05	556	0.86 ± 0.1	0.85 ± 0.5%
3	CH$_3$CN	540, 560	0.69 ± 0.1			
4[b]	THF	516	0.34			1.6

[a] The emission spectra were obtained from degassed solutions by exciting into the lowest MLCT band. [b] Values from ref 26.
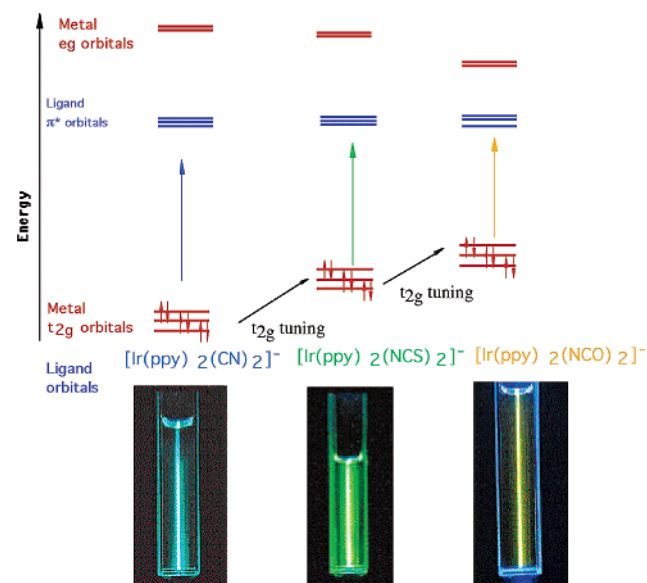

Figure 3. Schematic drawing of HOMO and LUMO orbitals for complexes **1**−**3** and their photoluminescence properties, which were obtained by exciting at 415.4 nm using a krypton ion laser.

1−**4**. The difference in the emission maxima is due to the difference in the ligand field strength of the pseudohalogen ligands. The photoluminescence obtained by exciting at 415.4 nm using a krypton ion laser is presented in Figure 3. It is apparent from the figure that complexes **1**, **2**, and **3** show a brilliant blue, green, and yellow luminescence, respectively.
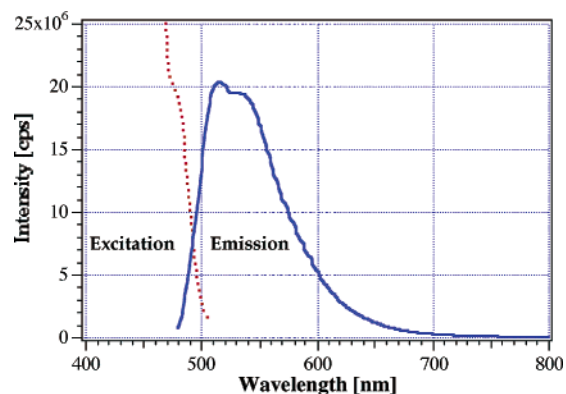
Figure 4. Emission and excitation spectra of complex **2** in dichloromethane solution at 298 K.

The iridium complexes **1**−**3** display unusual phosphorescence quantum yields in solution at room temperature, which is due to meticulous selection of the ligands that have higher ligand field strength. Introducing ligands such as CN$^-$ increases the gap between lowest unoccupied molecular orbital levels (LUMO) of the phenyl pyridine ligand and the metal t$_{2g}$ orbitals, resulting in a blue shift of the lowest MLCT and the emission maxima. Moreover, the gap between the LUMO of the phenyl pyridine ligand and the metal empty e$_g$ orbitals effectively increases because of the strong ligand field strength of cyanide ligands prohibiting nonradiative pathways, leading to 97% quantum yields in solution at room temperature with long lifetimes (Table 2, Figure 3).

The emission spectra of these complexes were measured in dichloromethane and acetonitrile solvents at 298 K and the data are collected in Table 2. The emission quantum yields are independent of the temperature variation. The emission spectral profile is independent of excitation wavelength and the excitation spectra matches well with the absorption spectra (Figure 4). In all these complexes the emission decayed as a single exponential with lifetimes of 0.8−3.4 μs in degassed CH$_2$Cl$_2$ solution, where the origin of the emitting state is the same. These lifetimes are indicative of strong spin−orbit coupling leading to intersystem crossing from the singlet to the triplet state. Hence, we believe that in these complexes the emission originates from the triplet states.[34]

Orthometalated iridium complexes are known to have the highest triplet quantum yields due to several factors: (a) Iridium has large d-orbital splitting compared to other metals in the series. (b) The strong ligand field strength of phenyl anion ligand increases the energy between the t$_{2g}$ and e$_g$ orbitals, leading to an enhanced gap between the e$_g$ and LUMO of the ligand. (c) Close lying π−π* and MLCT states together with the heavy atom effect enhance the spin−orbit coupling. An even more effective strategy to magnify the quantum yields of this class of complexes is to increase further the gap between the e$_g$ and LUMO orbitals by introducing the ligands such as CN$^-$, NCS$^-$, and NCO$^-$, which are known to have strong ligand field stabilization energy. In such type of complexes, the charge-transfer excited states decay through radiative pathways. The quantum yield data of complexes **1**−**3**, which were measured using recrystallized quinine sulfate in 1 N H$_2$SO$_4$ as a quantum

(34) Ichimura, K.; Kobayashi, T.; King, K. A.; Watts, R. J. *J. Phys. Chem.* **1987**, *91*, 6104.
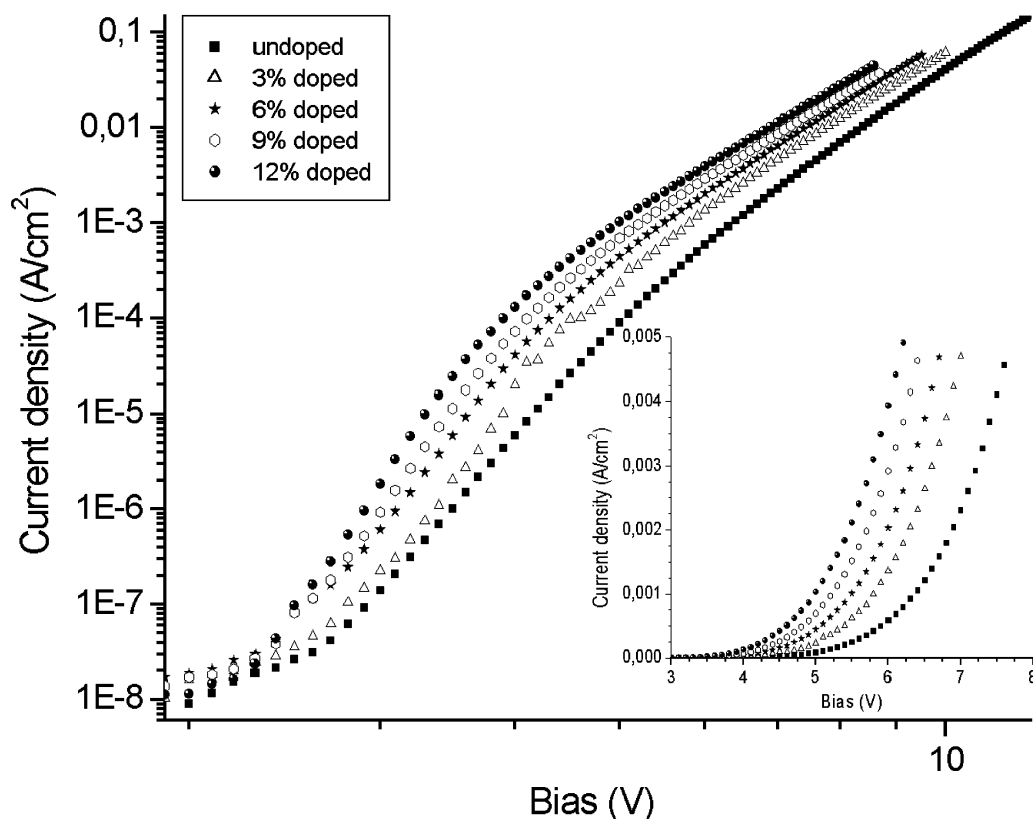
Figure 5. Current versus voltage as a function of doping concentration of the phosphorescent dye (ppy)$_2$Ir(acac) in a CBP matrix. In the inset, the same on a linear scale is presented.

yield standard, are collected in Table 2. At the same time a widely referred sample, Ru(bpy)$_3$(PF$_6$)$_2$, was used as a secondary standard to verify the yields obtained with quinine sulfate. The data obtained using both the standards are in excellent agreement and indeed show yields remarkably close to unity. The anionic complexes **1**−**3** are unprecedented in that they exhibit emission quantum efficiencies approaching one.

Up to now, most strategies to tune the photophysical properties of the phenylpyridine-based iridium complexes have been substitution of donor and/or acceptor groups on the pyridine and/or the phenyl groups.[23,35] However, the quantum yields in these complexes remained in the same range as the tris-phenylpyridine iridium(III) complex. This is not surprising, because the substitution of donor and/or acceptor groups tunes both the lowest unoccupied molecular orbitals (LUMO) and the highest occupied molecular orbitals (HOMO) levels of the metal complex in parallel, leading to marginal changes in the photophysical properties. On the other hand, in the case of mixed ligand complexes such as **1**, the LUMO level remained the same as phenylpyridine. Nevertheless, the HOMO level has stabilized significantly compared to tris-phenylpyridine iridium(III) complex, leading to a blue shift of the emission maxima, which is evident from the electrochemical data (Table 1). Therefore, this class of compounds provides an exciting opportunity to tune the emission spectral properties from blue to red by simply selecting appropriate donor/acceptor spectator ligands.

3.7. Organic Light-Emitting Device. Figure 5 shows the different current−voltage [I(V)] characteristics for complex **4**

(35) Grushin, V. V.; Herron, N.; LeCloux, D. D.; Marshall, W. J.; Petrov, V. A.; Wang, Y. *Chem. Commun.* **2001**, 2494.

Table 3. I(V) Characteristics as a Function of the Doping Rate of Complex **4** in a CBP Matrix[a]

doping rate	U_{th1}, V	exponent x_1: from $J = 3 \times 10^{-8}$ to 1×10^{-4} A/cm^2	U_{th2}, V	exponent x_2: $J > 1 \times 10^{-4}$ A/cm^2
undoped	3.5	12.7	11.1	8.0
3%	3.35	13.4	10.5	7.5
6%	3.1	14.7	10.0	7.4
9%	3.0	16.1	9.75	7.0
12%	2.9	16.9	9.4	6.8

[a] U_{th1} is defined for 1 μA/cm^2 and U_{th2} is defined for 0.1 A/cm^2.

doped in CBP host for various doping concentrations ranging from zero to 12 mol %. The voltage region below ∼2.5−3 V is characterized by a single carrier type transport, and the exact value depends on the doping concentration. Above this threshold voltage, we observe a steep increase in the diode current corresponding to two-carrier injection, which leads to light generation. We found, that the lower current threshold field (U_{th1}), here defined as the voltage for a current of 1 μA/cm^2, decreases monotonically from 3.5 V for the undoped case to 2.9 V for the maximum doped case of 12 mol % (see Table 3). This indicates that the dye molecules seem to improve carrier injection into the matrix layer. The energy barrier for holes at the α-NPD/CBP interface is 0.43 eV (HOMO−HOMO barrier). However, the energy barrier from α-NPD to complex **4** is negligible, which is less than 0.1 eV [cyclovoltametric measurements were done in our laboratory: HOMO's of α-NPD = 5.53 eV, CBP = 5.96 eV, and of complex **4** = 5.6 eV]. For higher doping concentrations, this injection and transport mechanism is even improved. The energy barriers for the

electrons are less important for the organic/organic interfaces (≤ 0.2 eV) until α-NPD, where they get blocked at the 0.6 eV barrier.

As the doping concentration increases, the edge in the $I(V)$ curve at around 1×10^{-4} A/cm^2 gets more visible. This edge marks the transition between two kinds of transport behavior as the applied electric field increases. At the lower current side of the edge ($J < 1 \times 10^{-4}$ A/cm^2) an increase of the steepness of the $I(V)$ line for increasing doping ratio is seen. For better interpretation we determined the power-law exponent ($I \approx U^{x_{1,2}}$) of the $I(V)$ lines, and the results are presented in Table 3. This increase of the exponent x_1 can be interpreted as injection improvement at the α-NPD/complex **4** interface. This interface can therefore be considered as the transport-limiting factor in the considered current range. Also, the upper current threshold field (U_{th2}), here defined as the voltage for a current of 100 mA/cm^2, decreases monotonically from 11.1 V for the undoped case to 9.4 V for the maximal doped case of 12 mol %. But contrary to this, the power-law exponent x_2 of the current (voltage) curve above the current edge decreases slightly, indicating a small deterioration of the total charge transport behavior in this current (voltage) range. Such a change can arise from a dopant-induced increase in the trap density accompanied by a lowering of the mobility, resulting in an increase of space charges screening in some way the applied electric field.[36]

It is necessary to introduce a hole-blocking layer (HBL) into our diode composition to confine the recombination zone inside the doped CBP layer; without the HBL the recombination takes place inside the Alq$_3$ layer (emission maximum at 530 nm wavelength). This indicates that with HBL the emission takes place in CBP just near the CBP/BCP interface as the electron are entering CBP. Alq$_3$ used as the standard matrix material for luminescent dyes cannot be used for complex **4**, because its band gap is too small to allow for an effective energy transfer rate from the host to the dye via Förster transfer.[37] By this mechanism the transfer rate is in principle proportional to the overlap of the emission spectra of the host and the absorption spectra of the dye, which is negligible for Alq$_3$ and complex **4**.

The doping with well-selected dye molecules into the emission matrix of an OLED results not only in a red shift of the emitted wavelengths but also in a considerable increase of the quantum efficiency. For a long time people thought that the luminescent dyes used since the discovery by Tang et al. are theoretically limited to an internal conversion efficiency of 25%.[38] This factor arrives from the quantum mechanics, where 75% of the charge wave functions are of the nonemissive triplet case and only 25% of the singlet case, allowing radiate recombination. Taking into account that only one-fifth of the created photon can leave the device, the external quantum efficiency was limited to 5%.[39] But in contrary to this, the complex **4** permits the opening of an additional radiative recombination channel because of spin–orbit coupling, resulting in a harvesting of up to nearly 100% of the exited states to photon creation. Taking into account an unchanged out coupling factor of one-fifth, the theoretical external quantum efficiency
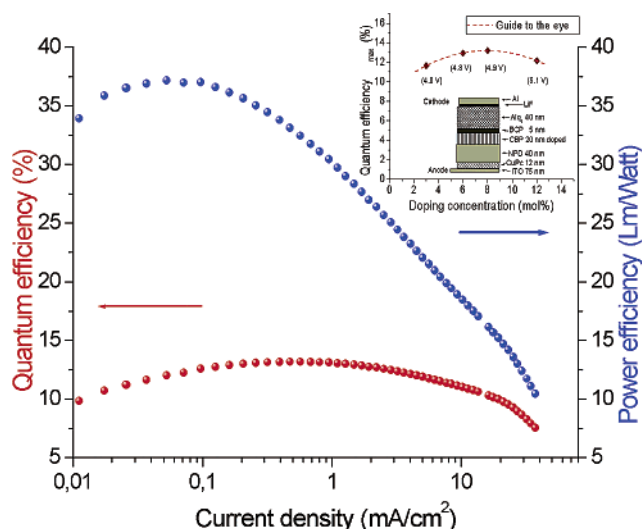

Figure 6. Quantum and power efficiency versus current using the complex [Ir(ppy)$_2$(acac)] (**4**). In the inset, the quantum efficiency as a function of the doping concentration of the complex **4** is presented.

now jumps up to 20%. In our case the maximum value of the experimental quantum efficiency increases from 0.94% for the undoped case up to 13.2% for the 9 mol % doped case, which is an improvement of more than 1 order of magnitude. Still more impressive is the improvement for the power efficiency, which increases from 0.65 to 37 lm/W, which represents a factor of 56.

These values are close to the values cited in the recent literature.[40] However, they are lower than the best values achieved with triplet emitters in TAZ host.[41] For a better comparison, the same architecture was used for the undoped case, including the BCP hole-blocking layer of 5 nm. This impressive value of quantum efficiency necessities also well-balanced charge relations inside the emission layer, without any current leaking either to the anode or to the cathode. Prior experiments showed us the way to get two extended well-working electrodes, with ITO/CuPc and LiF/Al, which provides an obviously good charge balance, taking into account the hole-blocking capabilities of BCP and the electron-blocking capabilities of α-NPD.[42–46] Another characteristic of phosphorescent dye doped OLED is that the maximum of the external quantum efficiency (QE) is located at low voltages (4.8 V) and that for higher voltages a strong decrease in the QE is seen. This kind of decrease is discussed as arising from a triplet–triplet annihilation effect.[47,48]

An advantage of the family of triplet emitters (complex **4**) is the large effective doping concentration range from low doping

(36) Jain, S. C.; Geens, W.; Mehra, A.; Kumar, V.; Aernouts, T. *J. Appl. Phys.* **2001**, *89*, 3804.
(37) Turo, N. J. *Modern Molecular Photochemistry*, University Science Books: Mill Valley, CA, 1991.
(38) Tang, C. W.; Van Slyke, S. A. *Appl. Phys. Lett.* **1987**, *51*, 913.
(39) Kim, J. S.; Ho, P. K. H.; Greenham, N. C.; Friend, R. H. *J. Appl. Phys.* **2000**, *88*, 1073.
(40) Lamansky, S.; Djurovich, P.; Murphy, D.; Abdel-Razzaq, F.; Lee, H. E.; Adachi, C.; Forrest, S. R.; Thompson, M. E. *J. Am. Chem. Soc.* **2001**, *123*, 4304.
(41) Adachi, C.; Baldo, M. A.; Thompson, M. E.; Forrest, S. R. *J. Appl. Phys.* **2001**, *90*, 5048.
(42) Masenelli, J. B.; Berner, D.; Bussac, M. N.; Nüesch, F.; Zuppiroli, L. *Appl. Phys. Lett.* **2001**, *79*, 4438.
(43) Nüesch, F.; Carrara, M.; Schaer, M.; Romero, D. B.; Zuppiroli, L. *Chem. Phys. Lett.* **2001**, *347*, 311.
(44) Tutis, E.; Bussac, M. N.; Masenelli, B.; Carrard, M.; Zuppiroli, L. *J. Appl. Phys.* **2001**, *89*, 430.
(45) Masenelli, B.; Tutis, E.; Bussac, M. N.; Zuppiroli, L. *Synth. Met.* **2001**, *122*, 141.
(46) Masenelli, B.; Tutis, E.; Bussac, M. N.; Zuppiroli, L. *Synth. Met.* **2001**, *121*, 1513.
(47) Hertel, D.; Romanovskii, Y. V.; Schweitzer, B.; Scherf, U.; Bässler, H. *J. Synth. Met.* **2001**, *116*, 139.
(48) Murata, H.; Merritt, C. D.; Kafafi, Z. H. *J. Selected Top. Quantum Electron.* **1998**, *4*, 119.
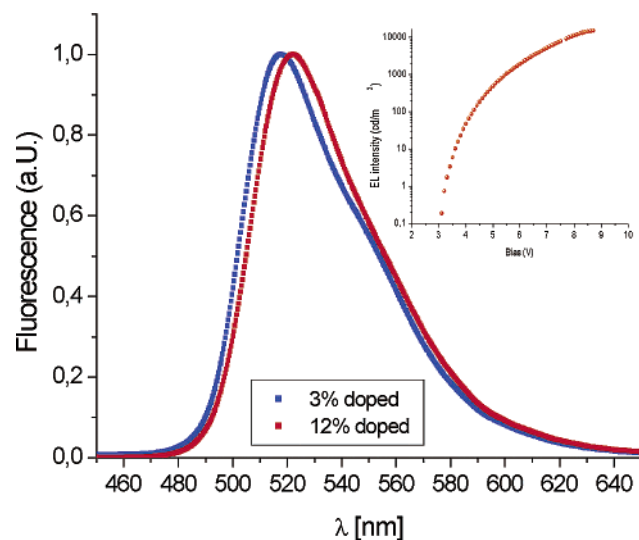
Figure 7. Electrophosphorescence of complex **4** in a CBP matrix for two doping concentrations. Additionally, the luminosity versus voltage is presented for the 9% doped case.

Table 4. Summary of Operating Conditions of Complex **4** in a CBP Matrix

doping rate	bias, V		
	at 100 cd/m^2	at 1000 cd/m^2	at 10000 cd/m^2
undoped	8.1	10.9	
3%	5.2	6.9	~10.1
6%	4.7	6.2	~9.5
9%	4.4	5.8	8.7
12%	4.4	5.8	8.7

concentrations up to more than 12 mol % without a significant change in the quantum efficiency (see the inset in Figure 6). In comparison, the quantum efficiency dependence on doping concentration of singlet emitters (e.g., rubrene, quinacridone, coumarin) is much more pronounced and the maximum is mostly located between doping ratios of 0.5 and 2 mol %.[48,49]

The electrophosphorescence intensity as a function of the voltage is shown for the 9% case in the inset of Figure 7. Table 4 shows a summary of the operating conditions for all the investigated devices. With increasing doping concentration the voltage to achieve a defined brightness decreases, which reflects well the change of the *I*(*V*) characteristic upon only a slightly change of the quantum efficiency.

Figure 7 shows the electrophosphorescence spectra of complex **4** for 3% and 12% doped in CBP. However, a slightly red shift for increasing doping concentration is seen, but the emission spectra was independent for current densities up to 150 mA/cm^2. Such a red shift as a function of the doping concentration was seen for DCM2, even if there the effect is much bigger.[50] In this publication the red shift was attributed to a polarization effect of the molecule introduced from the matrix, but then it should also be slightly current dependent, which it is not in our case. It is evident from Figure 7 that all the emitted light comes directly from the complex **4** molecules. The same emission peak is found from a solution phosphorescence spectra of complex **4**. Also, the emission peaks of α-NPD and the host, which are located in the blue around 440–450 and 480 nm, or intermediate exciplexes are not present. Another characteristic of phosphorescent dyes is the considerable reduction of the line width of the emitted spectra compared to standard luminescence materials such as Alq$_3$. In our case, the line width (fwhm) of the triplet emitter is only 52 nm in comparison with the line width of 83 nm of undoped Alq$_3$ emission, which leads to the saturated color that is necessary for high performance color displays, in assumption that the emission maximum is well located around one of the primary colors, green, blue, or red.

(49) Shoustikov, A. A.; You, Y.; Thompson, M. E. *Shoustikov, A. A.; You, Y.; Thompson, M. E., J. Selected Top. Quantum Electron.* **1998**, 4, 1998.

(50) Bulovi, V.; Shoustikov, A.; Baldo, M. A.; Bose, E.; Kozlov, V. G.; Thompson, M. E.; Forrest, S. R. *Chem. Phys. Lett.* **1998**, *287*, 455.